IEEE Access
Multidisciplinary | Rapid Review | Open Access Journal

Received 24 April 2024, accepted 14 May 2024, date of publication 20 May 2024, date of current version 3 June 2024.

Digital Object Identifier 10.1109/ACCESS.2024.3403207

RESEARCH ARTICLE

Hardware Implementation of a Solar-Powered Buck-Boost Converter for Enhanced Cathodic Protection Using Texas Instruments C2000 Board

AREZKI FEKIK[1,2], MIROSLAV MAHDAL[3], MOHAMED LAMINE HAMIDA[4], MALEK GHANES[2], (Member, IEEE), SUNDARAPANDIAN VAIDYANATHAN[5,6], AMAR BOUSBAINE[7], AND HAKIM DENOUN[4]

[1]Department of Electrical Engineering, Akli Mohand Oulhadj University of Bouria, Bouira 10000, Algeria
[2]LS2N, CNRS, École Centrale Nantes, UMR 6004, Nantes Université, 44000 Nantes, France
[3]Department of Control Systems and Instrumentation, Faculty of Mechanical Engineering, VSB—Technical University of Ostrava, 70800 Ostrava, Czech Republic
[4]Electrical Engineering Advanced Technology Laboratory (LATAGE), Tizi Ouzou 15000, Algeria
[5]Centre for Control Systems, Vel Tech University, Avadi, Chennai, Tamil Nadu 600062, India
[6]Centre of Excellence for Research, Value Innovation and Entrepreneurship (CERVIE), UCSI University, Cheras, Kuala Lumpur 56000, Malaysia
[7]College of Science and Engineering, University of Derby, DE22 3AW Derby, U.K.

Corresponding author: Sundarapandian Vaidyanathan (sundar@veltech.edu.in)

This work was supported in part by the European Union under the REFRESH–Research Excellence For REgion Sustainability and High-Tech Industries via the Operational Program Just Transition under Project CZ.10.03.01/00/22_003/0000048.

ABSTRACT This article delves into the hardware implementation of a buck-boost converter on a Texas Instruments C2000 board, tailored for impressed current cathodic protection to safeguard submerged metal structures against corrosion. Impressed current cathodic protection is vital for combating corrosion in buried or submerged metal structures, where a reliable power supply is crucial. The use of solar energy captured by photovoltaic panels emerges as an environmentally sustainable and economically viable solution for this critical application. The paper examines the design, hardware implementation, and system performance, focusing on the integration of the Texas Instruments C2000 board which is, pivotal for the automation and success of the impressed current cathodic protection system. The developed work aims to advance the sustainability of submerged metal structures by presenting a solution combining impressed current cathodic protection with the ecological advantages of solar energy.

INDEX TERMS Buck-boost converter, cathodic protection, closed loop control, C2000, Texas Instrument.

NOMENCLATURE

CP:	Cathodic Protection.
PV:	Photovoltaic.
PWM:	Pulse-Width Modulation.
MPPT:	Maximum Power Point Tracking.
P&O:	Perturb and Observe.
GPV:	Photovoltaic Generator.
MCU:	Microcontroller Unit.
I/O:	Digital Input and Output.
ADC:	Analog to Digital Converter.
TI:	Texas Instrument.
D:	Duty cycle.
I_{pv}:	Current output of a solar cell.
V_{pv}:	Voltage output of a solar cell.
Rp:	Parallel resistance.
Rs:	Series resistance.
q:	Charge of an electron.
I_{ph}:	Photocurrent of a diode.
Is:	Saturation current of a diode.
N:	Ideality factor of the diode.
K:	Boltzmann constant.

The associate editor coordinating the review of this manuscript and approving it for publication was Ahmed A. Zaki Diab.

T:	Temperature of a cell.
V_{pvm}:	Boost converter input voltage.
V_{dcm}:	Boost converter output voltage.
I_{Lm}:	Boost converter inductor current.
I_{dcm}:	Boost converter output current.
f_{sw}:	Boost converter switching frequency.
$V_{in} = V_{dcm}$:	Buck-boost converter input voltage.
V_{DC}:	Buck-boost converter output voltage.
V_L:	Buck-boost inductor voltage.
$I_{in} = I_{dcm}$:	Buck-boost converter input current.
I_{DC}:	Buck-boost converter output current.
I_L:	Buck-boost Inductor current.
I_C:	Buck-boost capacitor current.

I. INTRODUCTION

Cathodic protection (CP) is a fundamental discipline in the engineering and management of buried or submerged metallic infrastructures, such as pipelines, underground storage tanks, offshore platforms, and bridges. Its aim is to prevent corrosion, a natural process of metal degradation, by maintaining the electrical potential of structures at a sufficiently negative level to inhibit corrosion [1], [2], [3].

This field of research is highly relevant because the corrosion of metallic infrastructures can lead to significant economic, environmental, and safety damages. Electrical power supply is a critical component of cathodic protection, as it helps maintain the desired and constant electrical potential to extend the useful life of metallic infrastructures, minimize maintenance costs, and reduce the environmental impact of corrosion [4], [5]. In this context, the use of solar energy through photovoltaic panels offers a promising and eco-friendly alternative for powering cathodic protection systems, reducing reliance on traditional energy sources and contributing to a long-term infrastructure sustainability [6].

To ensure the efficacy of cathodic protection techniques, it is imperative to maintain a specific electrical potential on buried or submerged metallic structures, usually in the form of cathodic current. This constant electrical supply creates a favorable electrochemical environment that prevents corrosion. The stability of this power supply is crucial because the variations or interruptions in cathodic current can compromise the protection of the structure, leading to accelerated corrosion and potential safety risks for the infrastructure [7], [8].

The electrical power supply must also be adaptable to the environmental conditions and seasonal fluctuations, as cathodic current requirements can vary based on temperature, soil moisture, or the chemical composition of the surrounding environment. A reliable electrical power supply ensures the continuity of cathodic protection, resulting in substantial savings in terms of repair and replacement costs for metallic infrastructures and a reduction in environmental risks associated with corrosion.

Recent advancements in photovoltaic (PV) system the modeling of the series resistance (R_s) and shunt resistance (R_p) under partial shading conditions by [9], and converter analysis exemplified by the grid-interactive PV-fed BLDC pump with optimized MPPT in DC-DC converters explored by [10], pave the way for even more efficient integration of solar power into CP systems. Furthermore, research on solar photovoltaic converter controllers using novel optimization techniques, like the opposition-based reinforcement learning with butterfly optimization algorithm for partial shading conditions presented by [11], demonstrates the ongoing development of robust control strategies for these systems.

Solar energy, harnessed through photovoltaic panels, offers a promising and eco-friendly and sustainable solution for powering cathodic protection systems. The photovoltaic panels boast several advantages:

- Durability: They provide a long-lasting power source, minimizing maintenance needs.
- Environmental friendliness: Solar energy is a renewable resource, contributing to reduced greenhouse gas emissions and decreased dependence on fossil fuels.

In [12] a promising approach for MPPT in photovoltaic systems. Utilizing metaheuristic algorithms to optimize the FO-INC method enhances MPPT performance and maximizes the efficiency of PV systems.

Recent advancements in the field of renewable energy control systems, including the control and optimization of various renewable energy systems, are demonstrated in [13]. It also proposes novel circuits and systems to address nonlinear problems. Moreover, a comprehensive overview of various types of electronic power converters and their specific applications in renewable energy systems, such as solar, wind, and photovoltaic energy is presented in [14]. An optimized technique that utilizes a combination of the steepest gradient method and a step-size adaptation technique to enhance the performance of MPPT was presented in [15] and, [16] focuses broadly on the utilization of a multi-cell converter to optimize the MPPT of a solar panel that can provide more advantages compared to single-cell converters.

The fundamental objective of this article is to provide a detailed overview of the hardware implementation of a buck-boost converter specifically designed for the electrical power supply of cathodic protection systems, while highlighting the advantages of integration the Texas Instruments C2000 board. Cathodic protection is a vital technology for preserving metallic infrastructures and plays an essential role in corrosion prevention. However, a precise and reliable electrical power supply for these systems is a major challenge [14]. By leveraging solar energy through photovoltaic panels, this article explores a sustainable and cost-effective solution to meet this critical requirement. The ultimate goal is to provide engineers and researchers with a comprehensive reference for the design and successful implementation of cathodic protection systems powered by renewable energy sources, thus contributing to the sustainability of metallic infrastructures while reducing their environmental impact.

The innovative approach of this work lies in the, integration of solar energy to power the cathodic protection system.

This coupled with the development and validation of a tailored buck-boost converter for its self-power management and operation leading to an enhanced resilience of metallic infrastructures through experimental verification.

In order to provide a comprehensive exploration of the hardware implementation of a solar-powered buck-boost converter for enhanced cathodic protection using Texas Instruments C2000 Board, this paper is structured as follows:

Section II delves into the system's modeling, which encompass the modeling of PV cells, the design considerations for the Boost converters, and the implemented P&O MPPT strategies.

Section III elucidates the design and critical components selections for optimum operation of buck-boost converters.

Section IV presents, the exact sizing and modeling of cathodic protection system for optimal cathodic polarization potential of the pipeline.

Section V deals with the experimental work undertaken using TI C2000 for real-time control and command applications. The sections VI, VII and VIII illustrate the simulations, experimental results and a comprehensive conclusion respectively.

II. PV MODELING

The block diagram in Figure 1 represents the structure of the overall studied system, which is composed of three main parts: the power supply system, the cathodic protection buck-boost converter, and the model of the metallic structure (the load).

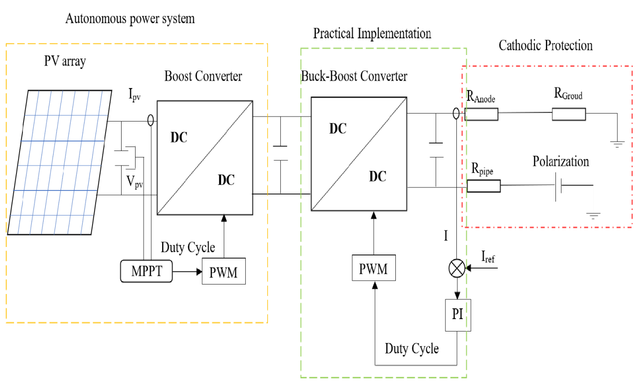

FIGURE 1. Global system control.

Figure 2 represents the equivalent circuit of a solar cell. The equivalent circuit of a cell consists of a current source in parallel with a diode, as well as a parallel resistance and a second series resistance. The mathematical model of the current generated by a photovoltaic cell is described by equation 1 [10], [11].

$$I_{pv} = \left(I_{ph} - I_s\left(\exp\left(\frac{q(V_{pv}+R_sI_{pv})}{NKT}\right)-1\right) - \frac{(V_{pv}+R_sI_{pv})}{R_p}\right) \quad (1)$$

where, I_{pv} and V_{pv} represent the current and voltage output of a solar cell, respectively:

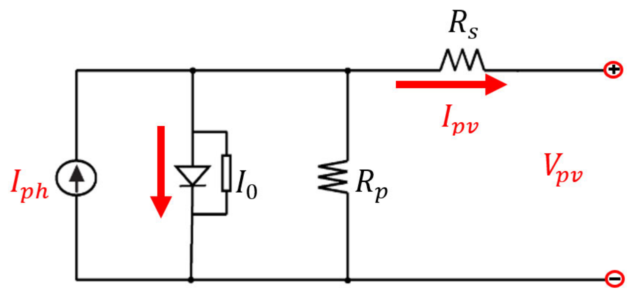

FIGURE 2. PV cell modeling.

R_p: is the parallel resistance, or shunt resistance, of a solar cell. In practice, the value of the resistance (R_p) is often high, so it can be neglected.

R_s: represents the series resistance.

q: is the charge of an electron (1.602×10^{-19} Coulombs).

I_{ph}: and I_s represent the photocurrent and the saturation current of a diode, respectively.

N: is the ideality factor of the diode.

K: is the Boltzmann constant (1.38×10^{-23} J/°K).

T: is the temperature of a cell.

A. BOOST CONVERTER

The BOOST converter, also known as a voltage step-up converter, can be represented by the circuit shown in Figure 3. [12]

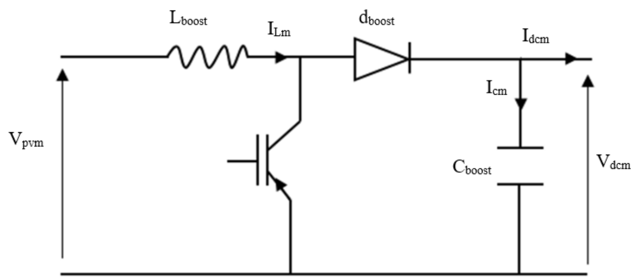

FIGURE 3. BOOST converter.

It is a direct DC-DC converter. The input source is a continuous current type (inductance in series with a voltage source), and the output load is a continuous voltage type (capacitor in parallel with the load).

The boost converter shown in Figure 3 is a popular form of converter made up of two energy storage components, the inductor L_{boost} and the capacitor C_{boost}. The inductor stores energy in a magnetic field during switch closure, and when the switch opens, it distributes energy to the load. The capacitor contributes to smoothing the output voltage and reducing ripples. The switch state changes between ON and OFF states in response to the control signal u. The ON state is in the time interval of $t \epsilon [0, DT]$, while the OFF state is in $t \epsilon [DT, (1-D)T]$, where D is the duty cycle. The duty cycle represents the ratio of time that the switch is closed to the entire switching periods [12].

- Switch On (u=1)

$$\begin{cases} V_{pvm} = L\dfrac{dI_L}{dt} \\ 0 = C\dfrac{dV_{dcm}}{dt} + I_{dcm} \end{cases} \tag{2}$$

- Switch Off (u=0)

$$\begin{cases} V_{pvm} = L\dfrac{dI_L}{dt} + V_{dcm} \\ I_{Lm} = C\dfrac{dV_{dcm}}{dt} + I_{dcm} \end{cases} \tag{3}$$

The two above-mentioned models of the converter, the continuous conduction mode (CCM) and the discontinuous conduction mode (DCM), can be gathered and represented in a single set of equations that describes the behavior of the converter under different operating conditions:

$$\begin{cases} V_{pvm} = L_{boost}\dfrac{dI_{Lm}}{dt} + (1-u) * V_{dcm} \\ I_{Lm} * (1-u) = C_{boost}\dfrac{dV_{dcm}}{dt} + I_{dcm} \end{cases} \tag{4}$$

By substituting variable u with its average value D (duty cycle) over a period T = 1/ f, where D is defined as the ratio of the time the switch is on (T_{ON}) to the total period (T), we can obtain the average model of the converter:

$$\begin{cases} V_{pvm} = L_{boost}\dfrac{dI_{Lm}}{dt} + \text{(1-D)} * V_{dcm} \\ I_{Lm} * (1-D) = C_{boost}\dfrac{dV_{dcm}}{dt} + I_{dcm} \end{cases} \tag{5}$$

The relationship between the average input voltage (V_{pvm}) and the average output voltage (V_{dcm}) is represented by the average inductor current (I_{Lm}) and the average output current (I_{dcm}). This relationship is important in understanding the performance of the system and making adjustments to optimize it. It can also be used to predict the behavior of the system under different conditions and to design new systems with improved performance:

$$V_{dcm} = \frac{1}{1-D}V_{pvm} \tag{6}$$

The dimensioning of inductance L is carried out based on the input current ripple. The inductance L is sized as follows:

$$L_{boost} \geq \frac{V_{pvm} * \text{(1-D)}\, D}{\Delta I f_{sw}} \tag{7}$$

The relationship that allows for sizing the capacitance C is given by:

$$C_{boost} \geq \frac{V_{pvm} * \text{(1-D)}\, D}{8 f_{sw}^2 L \Delta V} \tag{8}$$

With:

V_{pvm}: Boost converter input voltage
V_{dcm}: Boost converter output voltage.
I_{dcm}: Boost converter output current.
f_{sw}: Switching frequency of the boost converter.
D: The duty cycle.

B. MPPT CONTROL

The Perturb and Observe (P&O) method is widely used today due to its ease of implementation.

However, it presents some issues related to oscillations around the Maximum Power Point (MPP) it generates in steady-state operation. The search procedure for MPPT must be periodically repeated, forcing the system to continuously oscillate around the MPP once reached. These oscillations can be minimized by reducing the value of the perturbation variable. However, a small increment value slows down the search for MPP, so a balance must be found between accuracy and speed.

Figure 4 illustrates the classic algorithm associated with a Perturb and Observe (P&O) type Maximum Power Point Tracking (MPPT) control, where the power variation is analyzed after each voltage perturbation. For this type of control, two sensors (current and voltage of the Photovoltaic Generator - GPV) are necessary to determine the PV power at each moment [13].

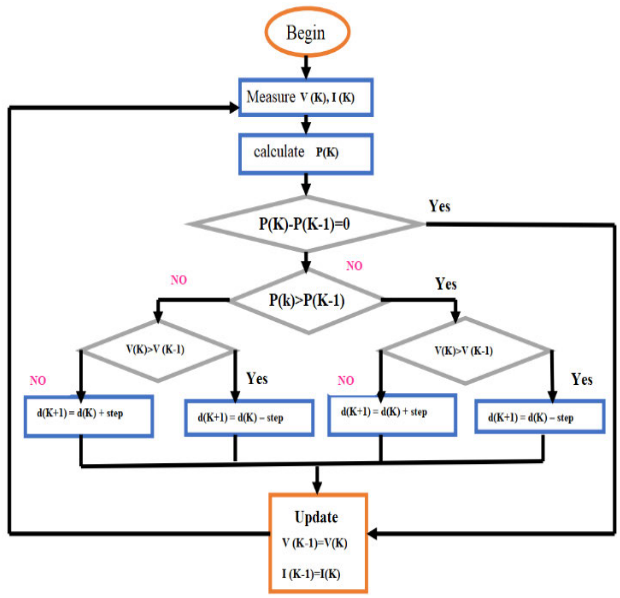

FIGURE 4. Typical algorithm of the Perturb and Observe (P&O) method.

This complicates the optimization of this control. We have developed a simulation model for the Perturb and Observe (P&O) algorithm, as depicted in Figure 5.

The output D of this algorithm is the duty cycle. ΔD is the perturbation value to be added and is set to 0.001. V and I are the voltage and current at the output of the PV array, respectively. P is the power generated by the PV array. Note that at the input of the MPPT block, voltage/current measurements should be used with a delay of 0.00001 s.

III. BUCK-BOOST CONVERTER

The Buck-Boost converter shown in the Figure 6 is a type of DC-DC converter that regulates the output voltage by providing an output voltage higher or lower than the input voltage, depending on the application's requirements. It combines the

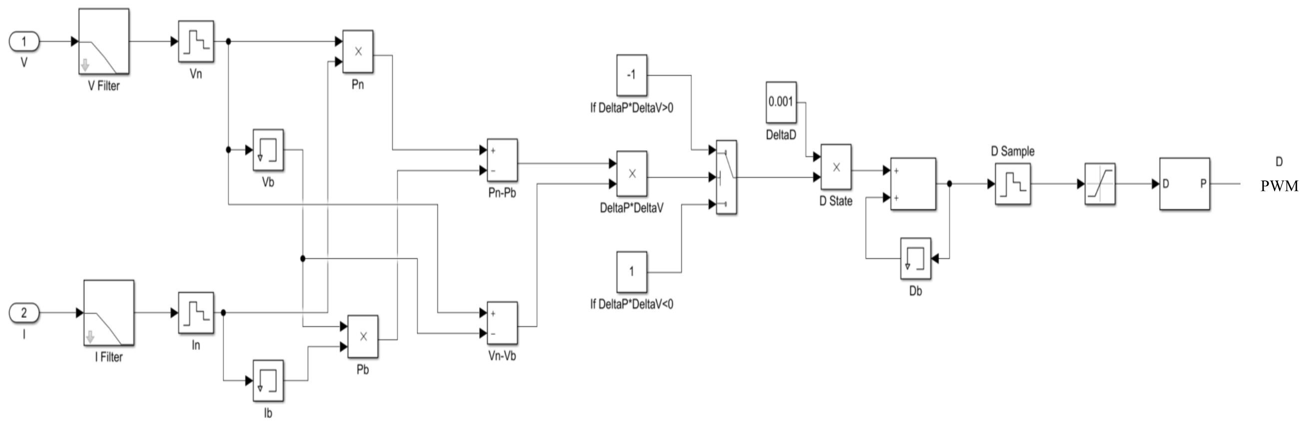

FIGURE 5. Functional simulation diagram of the Perturb and Observe (P&O) algorithm.

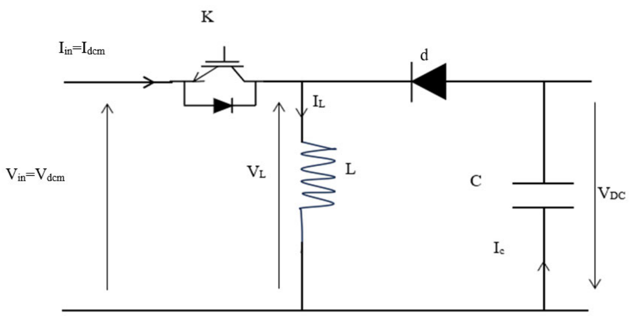

FIGURE 6. A basic schematic of the buck-boost converter.

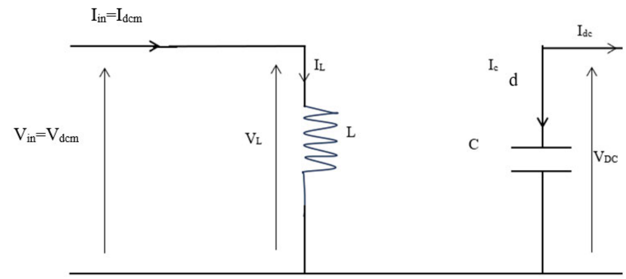

FIGURE 7. Structure of an equivalent circuit of the buck-boost converter during the on-state.

properties of both Buck and Boost converters and can thus be used as an ideal transformer to produce a required output voltage from an input voltage along a reverse polarity, diode for safe operation [15], [16], [17], [18].

There are, therefore, two possible configurations for the converter, and by applying Kirchhoff's laws to each the equations that define it can be extracted for the continuous conduction mode [19].

A. ON-STATE MODE OF OPERATION (SWITCH, K, CLOSED)

During this mode of operation, the switch K is ON for the duration of DT, where D is the duty cycle and T the time period.

By closing the switch, which offers zero resistance, the current flows, through the inductor and the switch and back to the DC input source. During this time, the inductor stores energy. When the diode is blocked, the polarity of the inductor reverses, allowing the current to flow through the load, and the diode before returning to the inductor. As a result, the direction of the current through the inductor remains unchanged [20].

By applying Kirchhoff's voltage law to the circuit, Figure 7 the following equations are obtained with the assumption that the devices are ideal [20]:

$$V_{in}\left(t\right) = V_L\left(t\right) \tag{9}$$

$$L\frac{di_L(t)}{dt} = V_{in}(t) \tag{10}$$

By integrating the differential equation (10), we get the solution as

$$i_L\left(t\right) = \frac{V_{in}}{L}t + I_{Lmin} \tag{11}$$

where at $t = 0$, minimum current is $i_{L(0)} = I_{Lmin}$, and at $t = DT$, the inductor current is at a maximal current I_{Lmax} under the steady state operation of the converter.

Therefore,

$$i_L\left(DT\right) = I_{Lmax} = \frac{V_{in}}{L}DT + I_{Lmin} \tag{12}$$

where the peak-to-peak ripple, Δi_L, of the current can be determined using the equation given below:

$$\Delta i_L = I_{Lmax} - I_{Lmin} = \frac{V_{in}}{L} * DT \text{ where } T = \frac{1}{f_s} \tag{13}$$

where:

$V_{in} = V_{dcm}$: buck-boost converter input voltage;
V_{DC}: buck-boost converter output voltage;
$V_L =$ buck-boost inductor voltage;
$I_{in} = I_{dcm}$: buck-boost converter input current;
I_{DC}: buck-boost converter output current;
I_L: buck-boost inductor current;
I_C: buck-boost capacitor current.

B. OFF-STATE MODE OF OPERATION (SWITCH, K, OPEN)

During the OFF cycle, DT to T, the diode D is conducting, as illustrated in Figure 8. During the current decay phase in

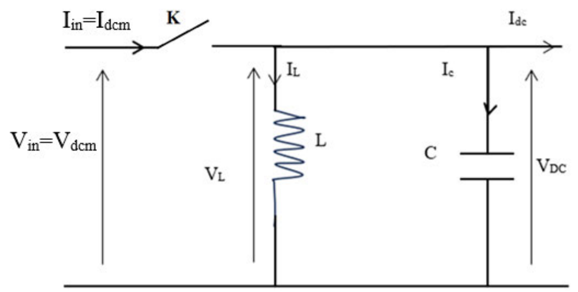

FIGURE 8. Equivalent circuit of the buck-boost converter during the OFF state.

inductor L, which corresponds to the opening of switch K, inductor L discharges and returns the energy it had previously stored to the load.

By applying Kirchhoff's voltage law to this circuit, the following equations are obtained [20]:

$$V_L(t) = -V_{DC}(t) \quad \text{with} \quad V_{DC}(t) = V_c(t) \tag{14}$$

$$V_L(t) = -L\frac{di_L(t)}{dt} = V_{DC}(t) \tag{15}$$

Solving using equations the same approach as during the ON state, the inductor current is given by

$$i_L(t) = \frac{V_{DC}}{L}t + I_{Lmax} \tag{16}$$

Also, the inductor current I_L, at t=T is given by the following equation:

$$i_L(T) = I_{Lmin} = \frac{-V_{DC}}{L}(T - DT) + I_{Lmax} \tag{17}$$

And the peak-to-peak ripple current Δi_L is determined by the following equation:

$$\Delta i_L = I_{Lmax} - I_{Lmin} = \frac{V_{DC}}{L}(\mathrm{T} - DT) \tag{18}$$

The duty cycle can be derived as follows:

$$\frac{V_{in}}{L}\mathrm{DT} = \frac{-V_{DC}}{L}(1 - D)T \rightarrow \frac{-V_{DC}}{V_{in} - V_{DC}} = D \tag{19}$$

Knowing that the output voltage is inverted, it can be written as

$$D = \frac{V_{DC}}{V_{in} + V_{DC}} \tag{20}$$

Also, the relationship between the input and the output of the converter is given as follows:

$$V_{DC} = \frac{\mathrm{D}}{1 - \mathrm{D}}V_{in} \tag{21}$$

The output voltage of the Buck-Boost converter is determined by the input voltage and the duty cycle D [20], [21], [22]. This converter can act as a step-down transformer for a duty cycle less than 0.5 or as a step-up transformer for a duty cycle greater than 0.5. However, since the output voltage is always of opposite polarity to the input voltage, it is often referred to as an inverting converter. The ideal output voltage is supposed to be independent of the load, but in practice, regulation must compensate for variations in input voltage and imperfections in real components.

C. CURRENT RIPPLE AND INDUCTOR SELECTION

The selection of the inductance for a Buck-Boost converter must be carefully considered to optimize efficiency, stability, and overall circuit performance. This can be done by using the previously defined equations [24], [25]:

The equation (22) relates the change in inductor current (Δi_L) to the direct current voltage (V_{DC}), the inductance (L), and the time period (T) minus the duty cycle times the time period (DT). The change in inductor current is essentially the difference between the maximum and minimum inductor currents.

$$\Delta i_L = I_{Lmax} - I_{Lmin} = \frac{V_{DC}}{L}(\mathrm{T} - DT) \tag{22}$$

This equation expresses the change in inductor current in terms of the direct current voltage (V_{DC}), the switching frequency (fs), the inductance (L), and the complement of the duty cycle (1 - D).

$$\Delta i_L = \frac{V_{DC}}{f_s L}(\text{1-D}) \tag{23}$$

The equation (23) can be solved for the inductance (L) in terms of the direct current voltage (V_{DC}), switching frequency (fs), change in inductor current (Δi_L), and the complement of the duty cycle (1 - D). The expression for V_{DC} is also given in terms of D/(1)-D) * V_{in}.

$$\mathrm{L} = \frac{V_{DC}}{f_s \Delta i_L}(\text{1-D}) \ \text{with} \ V_{DC} = \frac{\mathrm{D}}{1 - \mathrm{D}}V_{in} \tag{24}$$

Thus, we obtain the following:

$$\mathrm{L} = \frac{V_{in}}{f_s \Delta i_L}D \tag{25}$$

D. VOLTAGE RIPPLE AND CAPACITOR SELECTION

To choose the appropriate capacitor, it is generally recommended to start with a standard capacitor value and check if it meets the converter's specifications. If the voltage ripple is too high, a larger capacitor can be used to reduce the voltage ripple [24], [25]

By observing the current waveform presented in Figure 9, it is possible to determine the variation in voltage across the capacitor:

$$\Delta Q = \frac{-V_{DC}}{R}DT \tag{26}$$

This equation represents the change in charge (ΔQ) in a circuit element. It is equal to the negative of the product of

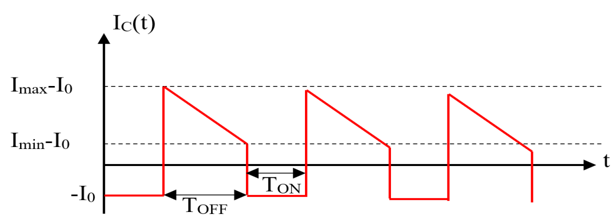

FIGURE 9. Current waveform across the capacitor.

the voltage across the element (V_{DC}) and the reciprocal of the resistance (R), multiplied by the change in time (DT).

$$|\Delta V_{DC}| = \frac{\Delta Q}{C} = \frac{V_{DC}}{RC} DT \tag{27}$$

This equation relates the absolute value of the change in output voltage ($|\Delta V_{DC}|$) to the change in charge (ΔQ) divided by the capacitance (C). It's also expressed in terms of the output voltage (V_{DC}), resistance (R), capacitance (C), and the change in time (DT).

$$C = \frac{V_{DC}}{R \Delta V_{DC} f_s} D \quad \text{with } V_{DC} = I_{DC} R \tag{28}$$

Here, C represents the capacitance, V_{DC} is the output voltage, R is the resistance, ΔV_{DC} is the change in output voltage, fs is the switching frequency, and D is the duty cycle. This equation provides a relationship between the capacitance, output voltage, resistance, change in output voltage, switching frequency, and duty cycle.

$$C = \frac{I_{DC}}{\Delta V_{DC} f_s} D \tag{29}$$

This equation expresses the capacitance in terms of the output current (I_{DC}), change in output voltage (ΔV_{DC}), switching frequency (fs), and duty cycle (D).

Based on the previously discussed equations, the sizing of the components was conducted, as illustrated in Table 1. It is worth noting that this approach differs from the conventional method of fixing the switching frequency (fs) and then searching for suitable components. Instead, the calculation of the appropriate frequency based on the available materials that were hand.

TABLE 1. Sizing of the regulation stages used in the system.

Converter	r	D	f_s	L_{min}	C_{min}	Δ_{i_L}	Δv_{DC}
Buck - Boost	$\frac{V_{DC}}{V_{in}}$	$\frac{V_{DC}}{V_{in}+V_{DC}}$	$\frac{R(1-D^2)}{2L}$	$\frac{V_{in}}{f_s \Delta i_L} D$	$\frac{I_{DC}}{\Delta V_{DC} f_s} D$	$\frac{V_{DC}}{f_s L}(1-D)$	$\frac{V_{DC}}{RC} DT$
	0.1	0.09	12KHz	300µH	10000µF	<15%	<1%

IV. MODELING OF THE LOAD

The exact sizing and modeling of cathodic protection fall within the expertise of a professional specialized in this field. However, it is appropriate to outline some fundamental principles for indicative purposes that will allow us to conduct the simulation.

In accordance with the presented circuit, it is easy to observe that the implementation of the entire circuit involves considering six resistances arranged in series [26].

$\mathbf{R^+}c$ and $\boldsymbol{Rc^-}$: These correspond to the resistance of the positive and negative cables. It depends on the length and cross-sectional area of the conductor. In theory, this resistance can be ignored.

$\boldsymbol{R_A}$: This is the anode-electrolyte resistance, which depends on the shape, number, and spacing of the anodes used, as well as the resistivity of the electrolyte.

$$R_A = \frac{0.00521\rho}{L}[\ln\left(\frac{8l}{\Delta}\right) - 1] \tag{30}$$

where ρ is the resistivity of the electrolyte (Ω.cm), and l and Δ are the length and diameter of the anode (cm).

$\boldsymbol{R_s}$: Represents the resistance of the structure to be protected (material) and is practically negligible.

$\boldsymbol{R}_{\mathrm{E}}$: This is the resistance of the electrolyte; each solution has a conductivity, resistivity, and resistance.

$\boldsymbol{R_v}$: Variable resistor placed to control the value of the applied current, following Ohm's law.

For the purpose of this study, we will represent only the load, estimated at 3.7 Ω, were made on the TFT site in Illizi in Algeria (estimated by DC R&D Sonatrach-Algeria), consisting of 3 resistances (anode, soil, structure) and the polarization potential of the pipeline, as shown in Table 2:

TABLE 2. Parameters of the equivalent circuit for the load.

Polarization P	R_{Anode}	R_{Sol}	$R_{Structure}$
0.85 V	1.5 Ω	1.5 Ω	0.7 Ω

It is estimated that a steel pipeline benefits from optimal cathodic protection when its potential, measured at any point relative to the Cu/CuSO4 reference electrode, remains below the threshold of −850 millivolts (corresponding to the immunity range of steel). This justifies the use of a polarization of 0.85V [27]. In other words, in case of system failure, the structures will have at least this potential.

V. EXPERIMENTATION

The C2000 board, developed by Texas Instruments, is an advanced hardware platform specifically designed for real-time control and command applications. It takes its name from the C2000 family of microcontrollers from Texas Instruments, which is widely used in a broad range of applications, including industrial automation, power electronics, embedded systems, and more.

A schematic of a typical control system based on C2000 is illustrated in Figure 11. The microcontroller is powered by a power supply system that accommodates primary voltage rails, including a 3.3 V analogue voltage (VDDA), a 3.3 V digital voltage (VDDIO), and a central 1.2 V power rail (VDD). The C2000 device provides rich peripheral support, and C2000-based systems typically consist of the following circuits connected to the MCU: power management, conditioning of analog input signals, quartz or external oscillator, reset circuits, communication transceivers, external interface to digital I/O pins, digital sensing, pulse-width modulation (PWM) interface/drivers, and any other required support circuitry [28].

To implement this system, we follow the steps for specific hardware configuration for the cathodic protection

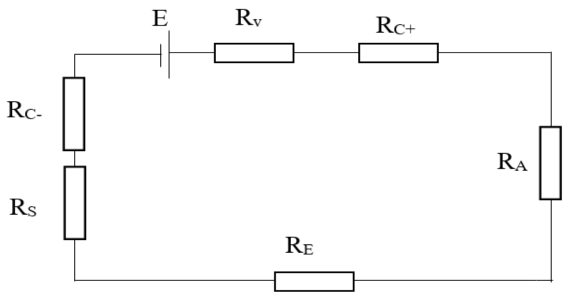

FIGURE 10. Simplified equivalent circuit of cathodic protection by impressed current.

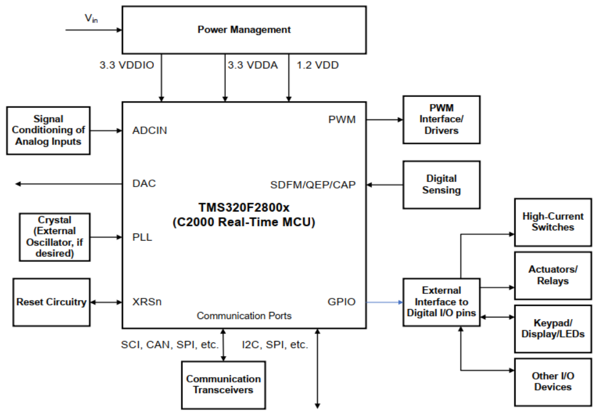

FIGURE 11. Typical C2000-based control system.

application with a buck-boost have been followed. In this application, there is an analogue input to measure the current at the output of the buck-boost and a PWM output to control the buck-boost.

A simple model that regulates the output current of a buck-boost converter to ensure proper cathodic protection has been created configured and designed to run on the TI Piccolo F28027 Launchpad. In the Simulink library browser, we add a new file and access the simulation settings to configure the board as shown in Figure 12.

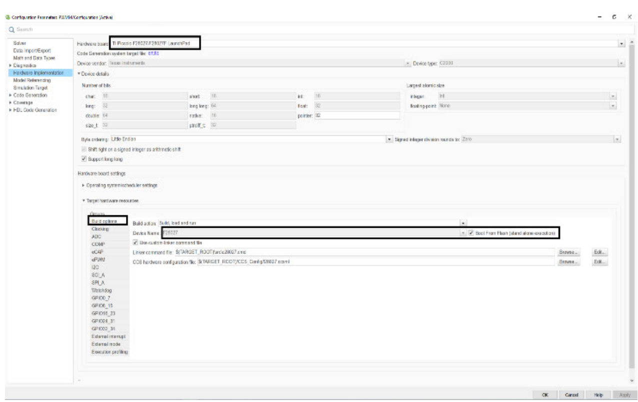

FIGURE 12. Selection of the C2000 board.

After selecting the board to be used (F28027 Launch Pad), we proceed to select the fixed-step calculation method and a discrete method as shown in Figure 13.

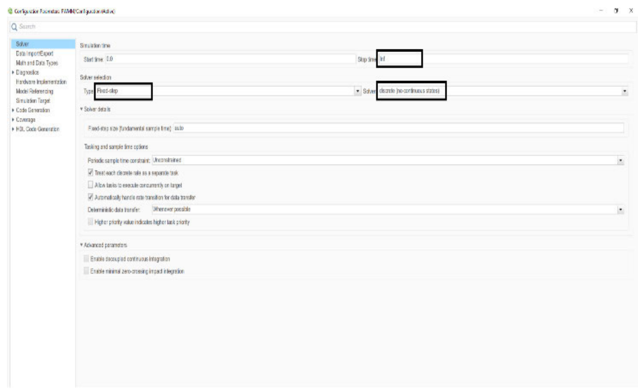

FIGURE 13. Selection of the C2000 board.

In the Libraries for C2000™ Microcontroller Blockset, we select the C2802x processor, then drag and drop the analogue-to-digital converter and PWM signal generation block as shown in Figure 14.

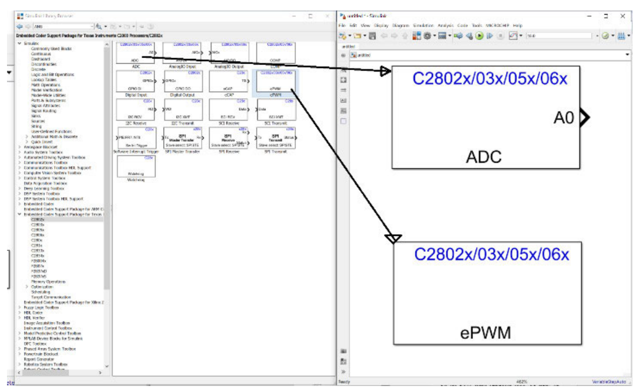

FIGURE 14. Selection of TI C2000 blocks.

To configure the two added blocks, we double-click on each block to open a dialog box. For the Analogue-to-Digital Converter block, select the parameters as shown in Figure 15.

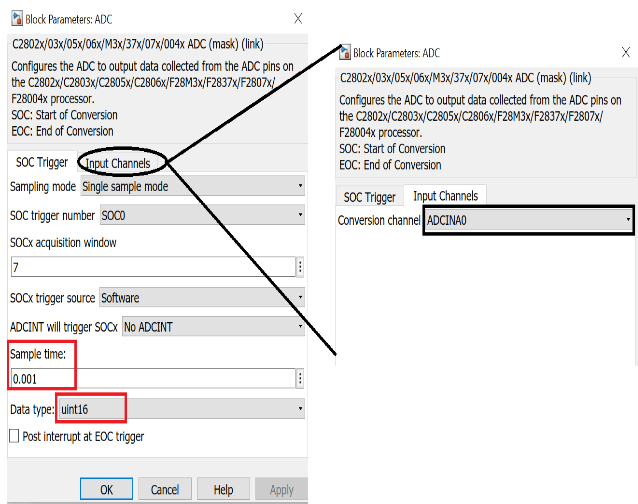

FIGURE 15. Configuration of the TI C2000 analog-to-digital converter block.

For the PWM Signal Generation block, we select the parameters as shown in Figure 16.

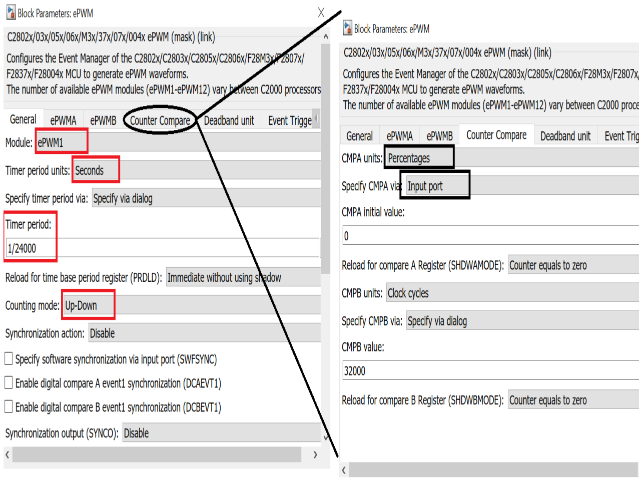

FIGURE 16. Configuration of the TI C2000 PWM block.

The block diagram of the hardware implementation on the Texas Instruments C2000 board for current regulation of a Buck-Boost converter is provided in Figure 17.

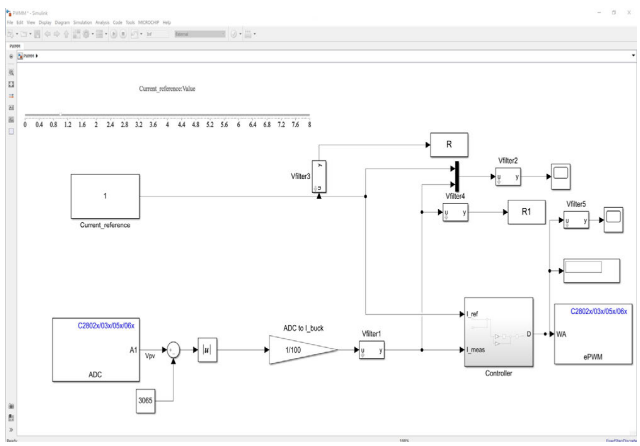

FIGURE 17. Closed-loop control block diagram with TI C2000.

VI. SIMULATION RESULTS

The closed-loop control of the Buck-Boost converter was simulated using Matlab/Simulink software, aiming to achieve current regulation with a target minimum of 10A. To assess the performance of the control strategy, a comprehensive numerical simulation was conducted within the MATLAB/Simulink environment, the results of which are depicted in Figures 18 and 19. Figure 18 provides an overview of various parameters associated with the Buck-Boost converter, emphasizing the regulation aspect. Notably, the simulation indicates that the regulatory mechanism is effective, as evidenced by the observed behaviour of the current delivered by the converter.

This behaviour is further elucidated in Figure 19, where the current delivered aligns closely with the reference current, converging steadily toward the desired value. The synchronization between the delivered current and the reference current, as indicated by the appropriate duty cycle, serves as confirmation of the successful implementation of the control strategy. The simulation results affirm the robustness and efficacy of the closed-loop control system, demonstrating its capability to regulate the current of the Buck-Boost converter in accordance with the specified target, thus validating the proposed control strategy.

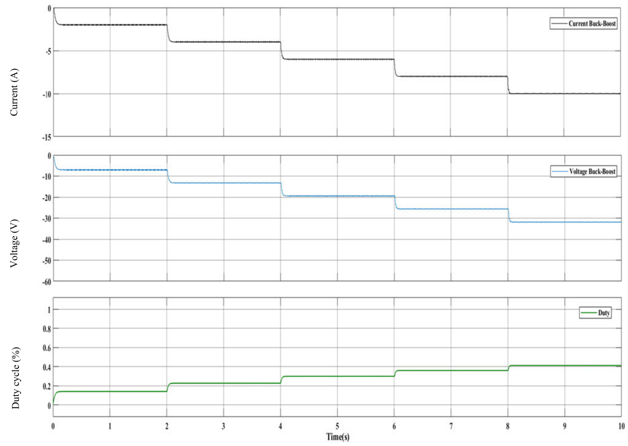

FIGURE 18. Parameters of the buck-boost stage with respect to regulation.

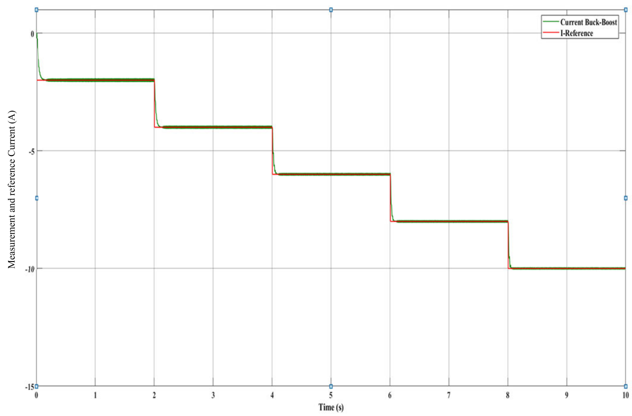

FIGURE 19. Current delivered by the buck-boost in relation to the reference current.

VII. EXPERIMENTAL RESULTS

Figure 20 shows a photograph of the test bench used for the control of the dedicated DC-DC Buck-Boost converter, specifically designed for the cathodic protection system.

The designed block consists of the following elements:

1. **Power Circuit:** This circuit is essentially the Buck-Boost converter, whose components were sized in accordance with the application.
2. **Control Circuit:** Comprising the Texas Instruments C2000 board.
3. **Driver Board:** Responsible for managing, controlling, and protecting power transistors, ensuring the optimal and safe operation of the converter.

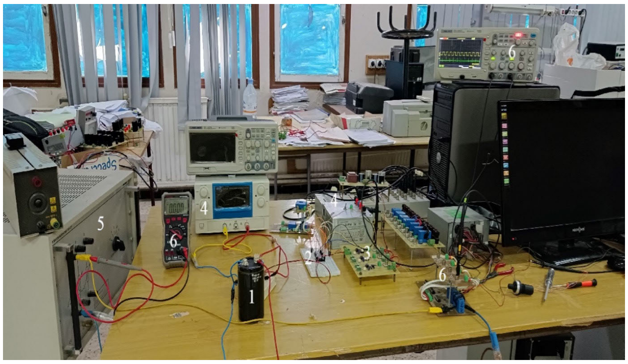

FIGURE 20. Test bench photograph.

4. **Stabilized Power Supplies:** A device designed to provide stable and regulated output voltage, independently of variations in input voltage or connected loads, to emulate the solar panel. They will be used to power different blocks of the system separately to create galvanic isolation where needed.
5. **Load:** It consists of a variable resistor with a fixed value of 6Ω (it is the value of the estimated resistance of the equivalent circuit namely (Ground Resistance, Anode Resistance and the resistance of the structure).
6. **Measurement and Visualization Equipment:** To measure and visualize the results obtained, an oscilloscope, a multimeter, and a current sensor LA-55A were used.

It should be noted that during experimental validation, for the photovoltaic system, an emulator is used to simulate the operation of the PV generator.

The Closed-loop control is one of the techniques used in control systems to achieve both static and dynamic performance. Controllers (PI, PID) are often combined between the setpoint and measurement to regulate the control, which is the duty cycle, especially the PWM signal applied to the converter.

The Texas Instruments C2000 board was used. This development board allows the adaptation the closed-loop control implementation in the simulation model developed in the MATLAB-Simulink environment to the experimental part. Using the TI C2000 Simulink library, one can easily generate PWM control signals without the need for programming.

It should be noted that the current sensor used has a factor of 0.12 V, as illustrated in the example in Figure 21(b). Observing a duty cycle of 40%, we can observe that the current displayed on the oscilloscope is 0.4. By performing the division 0.4/0.12, we obtain an output current equal to 3.33 A in absolute value.

The results obtained in Figures 21 and 22 experimentally can be summarized in Table 3, with V_{in} = 30V, which shows the comparison between the experimental and theoretically calculated results. It should be noted that the experimentation was stopped at a duty cycle of 60% because the power supply used can only deliver a maximum current of 15A.

FIGURE 21. Output parameters for a duty cycle of ((a): 30%), and ((b): 40%).

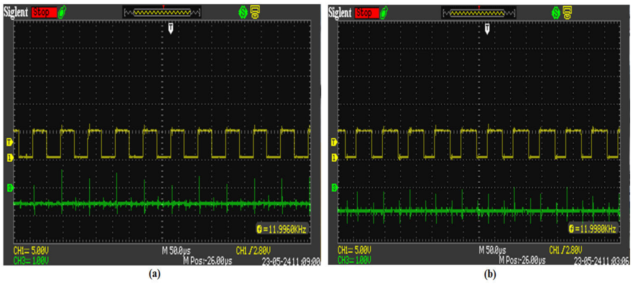

FIGURE 22. Output parameters for a duty cycle of ((a): 50%), and ((b): 60%).

Figures 21 and 22 represent the various experimental results obtained in closed-loop control for a duty cycle of 30% to 60%, respectively (depend of the variation of the current reference). Taking into consideration the losses inherent in the experimental environment and the components used, these results reveal a remarkable agreement and proportionality between theoretical values and experimental data, as evidenced by Table 3.

TABLE 3. Closed-loop experimental results.

D (%)	$V_{out} = \frac{D}{1-D} V_{in}$	R (Ω)	$I_{out_{Th}} = \frac{v_{out}}{R} = I_{ref}$	$\lvert v_{out} \rvert$	$\lvert I_{out} \rvert$
30	12.85	6	2.14	12.07	1.86
40	20	6	3.33	18.75	3.33
50	30	6	5	27.68	4 .6
60	45	6	7.5	44.36	7.16

Figure 23 shows that the measured current (the actual current obtained, absolute value) perfectly follows the reference for each variation of the current reference. This indicates that the PI current regulation is effective in maintaining the converter's output current as close as possible to the desired reference. The analysis of Figure 24 highlights the stable behavior of the buck-boost converter regulated by a PI controller, even when subjected to disturbances such as load variations. The results show that the measured current precisely follows the 2 A reference, with only slight transient response.

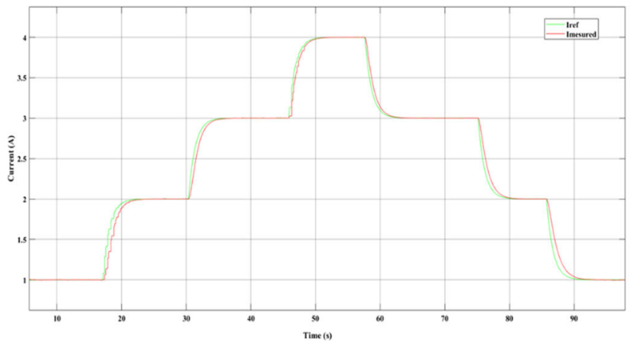

FIGURE 23. Measured current with current reference variation (Absolute value).

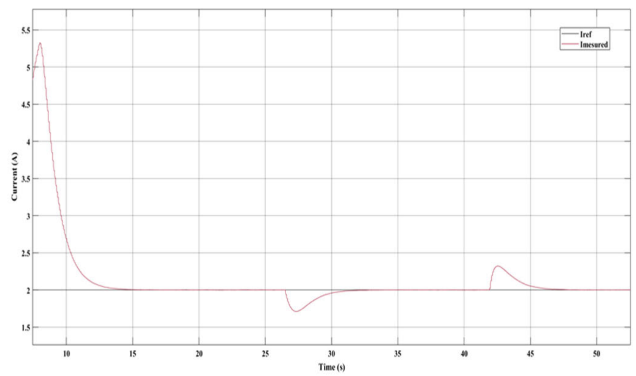

FIGURE 24. Measured current with load variation (absolute value).

VIII. CONCLUSION

The results show that the hardware implementation effectively regulates Buck-Boost converter output current for a reliable cathodic protection. A strong agreement between simulations, experiments, and theory the confirms robustness of the closed-loop control system developed. The Texas Instruments, C2000 platform proved valuable for the configuration and control, enabling rapid adaptation. This study validates a reliable and efficient cathodic protection system using solar power and a Buck-Boost converter on the Texas Instruments C2000 board, paving the way for wider adoption of this environmentally friendly solution.

REFERENCES

[1] R. Singh, *Corrosion Control for Offshore Structures: Cathodic Protection and High-Efficiency Coating*. Oxford, U.K.: Gulf Professional, 2014.

[2] S. Zehra, M. Mobin, and R. Aslam, "Corrosion prevention and protection methods," in *Eco-Friendly Corrosion Inhibitors*, L. Guo, C. Verma and D. Zhang, Eds. Berlin, Germany: Elsevier, 2022, pp. 13–26.

[3] R. T. Loto and C. A. Loto, "Corrosion and protection of facilities and infrastructures in telecommunications industry—A review," *IOP Conf. Ser., Mater. Sci. Eng.*, vol. 1107, no. 1, Apr. 2021, Art. no. 012014.

[4] J. Liu, X. Fang, C. Zhu, X. Xing, G. Cui, and Z. Li, "Fabrication of superhydrophobic coatings for corrosion protection by electrodeposition: A comprehensive review," *Colloids Surf. A, Physicochemical Eng. Aspects*, vol. 607, Dec. 2020, Art. no. 125498.

[5] S. V. Harb, A. Trentin, T. A. C. de Souza, M. Magnani, S. H. Pulcinelli, C. V. Santilli, and P. Hammer, "Effective corrosion protection by eco-friendly self-healing PMMA-cerium oxide coatings," *Chem. Eng. J.*, vol. 383, Mar. 2020, Art. no. 123219.

[6] S. O. Ganiyu and C. A. Martínez-Huitle, "The use of renewable energies driving electrochemical technologies for environmental applications," *Current Opinion Electrochem.*, vol. 22, pp. 211–220, Aug. 2020.

[7] N. Karabacak and A. Karakaya, "Using solar energy in galvanic anode cathodic protection systems," *Int. J. Energy Appl. Technol.*, vol. 10, no. 1, pp. 6–13, Jun. 2023.

[8] V. Liduino, M. Galvão, S. Brasil, and E. Sérvulo, "SRB-mediated corrosion of marine submerged AISI 1020 steel under impressed current cathodic protection," *Colloids Surf. B, Biointerfaces*, vol. 202, Jun. 2021, Art. no. 111701.

[9] H. Oufettoul, N. Lamdihine, S. Motahhir, N. Lamrini, I. A. Abdelmoula, and G. Aniba, "Comparative performance analysis of PV module positions in a solar PV array under partial shading conditions," *IEEE Access*, vol. 11, pp. 12176–12194, 2023.

[10] S. Murshid and B. Singh, "Single stage autonomous solar water pumping system using PMSM drive," *IEEE Trans. Ind. Appl.*, vol. 56, no. 4, pp. 3985–3994, Jul. 2020.

[11] B. Aljafari, P. K. Balachandran, D. Samithas, and S. B. Thanikanti, "Solar photovoltaic converter controller using opposition-based reinforcement learning with butterfly optimization algorithm under partial shading conditions," *Environ. Sci. Pollut. Res.*, vol. 30, no. 28, pp. 72617–72640, May 2023.

[12] H. H. Ammar, A. T. Azar, R. Shalaby, and M. I. Mahmoud, "Metaheuristic optimization of fractional order incremental conductance (FO-INC) maximum power point tracking (MPPT)," *Complexity*, vol. 2019, pp. 1–13, Nov. 2019.

[13] A. T. Azar and N. A. Kamal, *Renewable Energy Systems*. London, U.K.: Academic Press, 2021.

[14] A. Fekik, M. Ghanes, and H. Denoun, *Power Electronics Converters and Their Control for Renewable Energy Applications*. New York, NY, USA: Elsevier, 2023.

[15] K. Amara, T. Bakir, A. Malek, D. Hocine, E. B. Bourennane, A. Fekik, and M. Zaouia, "An optimized steepest gradient based maximum power point tracking for PV control systems," *Int. J. Electr. Eng. Informat.*, vol. 11, no. 4, pp. 662–683, Dec. 2019.

[16] A. Fekik, A. T. Azar, N. A. Kamal, F. E. Serrano, M. L. Hamida, H. Denoun, and N. Yassa, "Maximum power extraction from a photovoltaic panel connected to a multi-cell converter," in *Proc. Int. Conf. Adv. Intell. Syst. Inform.*, vol. 1261, Sep. 2020, pp. 873–882.

[17] D. O. Onuoha, C. E. Mgbemena, H. C. Godwin, and F. N. Okeagu, "Application of Industry 4.0 technologies for effective remote monitoring of cathodic protection system of oil and gas pipelines—A systematic review," *Int. J. Ind. Prod. Eng.*, vol. 1, no. 2, Nov. 2022, Art. no. 04104232.

[18] H. U. Rehman, N. Ahmed, H. A. Sher, A. Al-Durra, and H. M. Hasanien, "Comprehensive analysis and design of a switched-inductor type low inductance-requirement DC–DC buck-boost converter for low power applications," *IET Power Electron.*, vol. 16, no. 7, pp. 1239–1254, Feb. 2023.

[19] C. González-Castaño, C. Restrepo, F. Flores-Bahamonde, and J. Rodriguez, "A composite DC–DC converter based on the versatile buck–boost topology for electric vehicle applications," *Sensors*, vol. 22, no. 14, p. 5409, Jul. 2022.

[20] M. S. Khan, S. S. Nag, A. Das, and C. Yoon, "Analysis and control of an input-parallel output-series connected buck-boost DC–DC converter for electric vehicle powertrains," *IEEE Trans. Transport. Electrific.*, vol. 9, no. 2, pp. 2015–2025, Jun. 2023.

[21] A. Sarikhani, B. Allahverdinejad, and M. Hamzeh, "A nonisolated buck–boost DC–DC converter with continuous input current for photovoltaic applications," *IEEE J. Emerg. Sel. Topics Power Electron.*, vol. 9, no. 1, pp. 804–811, Feb. 2021.

[22] H. Afshari, O. Husev, and D. Vinnikov, "A novel isolated buck-boost DC–DC converter with wide range of voltage regulations," in *Proc. IEEE 17th Int. Conf. Compat., Power Electron. Power Eng. (CPE-POWERENG)*, Aug. 2023, pp. 1–6.

[23] A. Singh, J. Gupta, and B. Singh, "Design and control of two stage battery charger for low voltage electric vehicles using high gain buck-boost PFC AC–DC converter," *IEEE Trans. Ind. Appl.*, vol. 59, no. 5, pp. 6125–6135, Sep. 2023, doi: 10.1109/TIA.2023.3282612.

[24] J. C. Mayo-Maldonado, J. E. Valdez-Resendiz, P. M. Garcia-Vite, J. C. Rosas-Caro, M. del Rosario Rivera-Espinosa, and A. Valderrabano-Gonzalez, "Quadratic buck–boost converter with zero output voltage ripple at a selectable operating point," *IEEE Trans. Ind. Appl.*, vol. 55, no. 3, pp. 2813–2822, May 2019, doi: 10.1109/TIA.2018.2889421.

[25] J. C. Rosas-Caro, J. E. Valdez-Resendiz, J. C. Mayo-Maldonado, A. Alejo-Reyes, and A. Valderrabano-Gonzalez, "Quadratic buck–boost converter with positive output voltage and minimum ripple point design," *IET Power Electron.*, vol. 11, no. 7, pp. 1306–1313, Apr. 2018.

[26] J. C. Rosas-Caro, V. M. Sanchez, J. E. Valdez-Resendiz, J. C. Mayo-Maldonado, F. Beltran-Carbajal, and A. Valderrabano-Gonzalez, "Quadratic buck-boost converter with positive output-voltage and continuous input-current," in *Proc. Int. Conf. Electron., Commun. Comput. (CONIELECOMP)*, Feb. 2018, pp. 152–158.

[27] J. Lee, "Basic calculation of a buck converter's power stage," Richtek Technol. Corp., Dallas, TX, USA, Tech. Rep., AN041, 2015, pp. 1–8.

[28] S. D. Sudhoff, *Power Magnetic Devices: A Multi-Objective Design Approach*. New York, NY, USA: The Institute of Electrical and Electronics Engineers, Oct. 2022, doi: 10.1002/9781119674658.

AREZKI FEKIK is a Senior Lecturer with the Akli Mohand Oulhadj University of Bouira, Algeria. Currently, he performs the functions of design engineer supporting experimental tests and research in power systems control with the Laboratoire des Sciences Numérique de Nantes (LS2N), l'École Centrale de Nantes. He has published more than 65 journals and conference papers and book chapters in the fields of power electronics and its applications. His current research interests include power electronics and its applications, such as wind turbines, photovoltaic systems, reliability, harmonics, microgrids, and variable speed drives. He is a member of the International Group of System Control (IGCS), the Springer Conference Committee, and the IEEE SMARTTECH Conference.

MIROSLAV MAHDAL is currently a Vice-Dean for Science, Research, and Doctoral Studies with the Faculty of Mechanical Engineering, VSB—Technical University of Ostrava and an Associate Professor with the Department of Control Systems and Instrumentation. He has more than 80 articles to his credit. His research interests include control of mechatronic systems, control systems, automatic control theory, wireless technologies, artificial intelligence, cloud computing, optimization methods, and programming of control systems.

MOHAMED LAMINE HAMIDA received the B.Sc., M.Sc., and Ph.D. degrees in electrical engineering from Mouloud Mammeri University, Tizi Ouzou, Algeria, in 2013, 2015, and 2019, respectively. He has been a member of the Electrical Engineering Advanced Technology Laboratory (LATAGE), since 2015, and became a Lecturer, in 2020. He has published many journals and conference papers in the field of power electronics and its applications. His current research interests include power electronics and its applications, such as the application of PWM, fuzzy logic control, sliding mode control, and petri nets modeling to dc/d and dc/ac multicell converters.

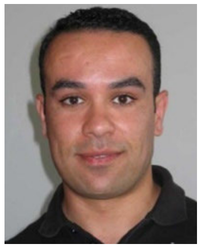

MALEK GHANES (Member, IEEE) received the M.Sc. and Ph.D. degrees in applied automatic and informatics from the Institut de Recherche en Communications et Cybernétique de Nantes (IRCCyN) (currently LS2N), Nantes, France, in 2002 and 2005, respectively. From September 2005 to 2006, he was a Postdoctoral Researcher with the Groupe de Recherche en Informatique, Image, Automatique et Instrumentation de Caen (GReyC). Since April 2016, he has been with the Électronique et Commande des Systémes (ECS) Laboratory, Quartz, École Nationale Supérieure de l'Électronique et de ses Applications (ENSEA), Cergy, France, where he was an Associate Professor and the Head of the Department of Automatic and Electrical Engineering. In May 2016, he was promoted as a Full Professor with LS2N-ECN. He is currently holding a Chair on electric vehicle performances between Renault and Centrale Nantes (CN). He has published more than 100 journals, conference papers, and several patents. His research interests include observation and control of nonlinear systems, with the applications to electric systems.

SUNDARAPANDIAN VAIDYANATHAN received the D.Sc. degree in electrical and systems engineering from Washington University in St. Louis, MO, USA, in May1996. He is currently a Professor and the Dean of the Centre for Control Systems, Vel Tech University, Avadi, Chennai, India. He is also a Distinguished Visiting Professor with the Centre of Excellence for Research, Value Innovation and Entrepreneurship (CERVIE), UCSI University, Kuala Lumpur, Malaysia. He has published over 600 Scopus-indexed research publications. His current research interests include linear and nonlinear control systems, chaotic and hyperchaotic systems, circuits, intelligent control, optimal control, mathematical modeling, and scientific computing.

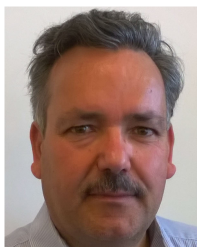

AMAR BOUSBAINE received the Ingenieur d'Etat (M.Eng.) degree in electro-technique from the University of Tizi Ouzou, Tizi Ouzou, Algeria, the M.Sc. degree in electrical power engineering from the University of Strathclyde, Glasgow, U.K., and the Ph.D. degree in thermal modeling of induction machines from The University of Sheffield, Sheffield, U.K. Previously, he was with the Electrical and Electronic Engineering Department, De Montfort University, as a Lecturer. He is currently with the College of Science and Engineering, University of Derby, Derby, U.K., as an Associate Professor in power electronics and automotive electrical systems. He is an active researcher in the fields of automotive electrical power system for electrical vehicles (EVs), renewable energy sources, hydrogen fuel cells, and autonomous control of drones. He draws upon a wealth of industrial experiences as a project leader for various industrially sponsored projects. He is a member of IET and HEA.

HAKIM DENOUN received the B.Sc. degree in electrical engineering from Mouloud Mammeri University, Algeria, the D.E.A. degree from Paris 6, France, the Magister degree from the Polytechnic School, Algiers, Algeria, and the Ph.D. degree in electrical engineering from Mouloud Mammeri University. He is currently a Professor with Mouloud Mammeri University. He is affiliated with the Electrical Engineering Advanced Technology Laboratory (LATAGE). His research interests include electrical machines and drives, power electronics, and control systems.